

RESEARCH ARTICLE

## Quantum Relativistic Proton Radiation Therapy of Eye Cancer with Injecting Gold Nanoparticles.

S. N. Hossenimotlagh

Department of Physics, Azad Islamic University, Shiraz Branch, Iran, Shiraz

### ABSTRACT

In this work, we use the comprehensive relativistic quantum theory of Bethe- Bloch model and Monte Carlo Geant4 / Gate simulations to calculate the dose distribution in the eye tumor using proton therapy with and without gold nanoparticles(GNPs) injection. The calculation results indicate an increase in the amount of deposited dose in the eye tumor due to the combination of gold nanoparticles with proton therapy. The use of GNPs during proton therapy is beneficial, because these nanoparticles, due to their optical resonance properties, release X-rays due to protons, and these x-rays are produced directly at the tumor site. This study shows that the selection of physical interactions models, variation of concentration injected GNPs, size of the nanoparticles, the selected phantom, size of the tumor, location of the tumor, energy and the geometry of incident proton beam, proton fluence are the basic parameters that affect on the total stopping power, dose distribution, range straggling and mean scattering angle in the eye tumor and not only the dose distribution but also the enhancement of dose, is related to the production of higher energy secondary electrons within the GNPs.

### INTRODUCTION

Proton therapy is basically a better form of treatment. Although X-rays can treat many cancers, the risk of damage to healthy tissues is high by them. For this reason, medical teams use less dose in treatment with X-rays, but in proton therapy they can be used more values of radiation dose, while harm to healthy tissues is much reduced. In addition, the other advantages of proton therapy are fewer side effects and faster improvement due to more accurate radiation exposure to targeted areas. When protons collide target, they perform electrostatic interactions with the atoms of the target through Coulombic force. As a result of these forces, some of the electrons are scattered and changed their directions or, in many cases, transfer part of their energy to the sample. When a proton passes near the electron circular orbit inside the target, the proton removes the electron from its orbit and causes the ionization of the target atom. This also changes the properties of the target atoms, and this phenomenon is beneficial for proton therapy. In proton therapy, a proton accelerator is used to expose the tumor using a proton beam. Because of the ionization of atoms within the cancer molecules by proton beam, the cancer cells are damaged and the DNA is hurt. Damaging the DNA causes the function of the cell division ability to be eliminated. Intracellular enzymes develop and try to rebuild DNA in those damaged areas, but enzymes can not improve damage if radiation damage is high and when both healthy and cancer cells want to repair the cell, the ability of cancer cells is far less than healthy cells, and therefore

Address for Correspondence: S. N. Hossenimotlagh, Department of Physics, Azad Islamic University, Shiraz Branch, Iran, Shiraz

### KEYWORDS

eye tumor, relativistic quantum, simulation, proton therapy, nanoparticles

### History

Received :18 January 2020  
Accepted :09 April 2020  
Published :29 June 2020

Volume :7 Issue : 1

cancer cells are involved in cell death or apoptosis. The history of proton therapy investigation back to 1946, when Wilson, at Harvard, proposed the use of accelerated proton in radiotherapy. Since then, the rate of progression of proton therapy has been slowed which probably due to technical problems, the required equipment, and its high cost. In 1954, Tobias et al. for the first time at Lawrence Berkeley Lab treated patients with proton radiation. In 1962, proton's specialized therapies began at Harvard's Cyclotron Laboratory by Cagliberger and et al., and it was followed in the mid-1970s by treating eye cancer and larger tumors and so far, many treatments have been made with proton therapy. Proton therapy can be used to treat almost all tumors that are commonly treated with x-rays or electrons. Such as tumors of the brain, ocular tumors, spinal cord, head and neck, eye, lung, gastrointestinal malignancies, prostate cancers, and so on. Heavy particles, including proton, have a unique property in terms of uniformity in the distribution of the dose in the target volume and the absence of an external dose for healthy tissues. [1] In fact, proton beams have a desirable dose of radio-therapy. With passing of charged particles in matter, the particle energy rate reduction in the unit length of the path due to ionization and excitation is created and directly proportional to the square of the charge particle and also proportional to its the inverse of square velocity. By reducing the energy of the particle, its velocity decreases and its reduction rate increases along the path. When the particle velocity approaches the zero at the end of its range, the reduction of energy rate is maximized. The depth-dose distribution follows the reduction of energy rate in the material. When a beam of protons enters the homogeneous tissue, stopping power rapidly increases

with decreasing proton energy. As a result, the deposited dose is increased because of slowing down the protons with a steep slope toward the end of the pathway of the protons. Diagram of absorbed dose changes based on the depth of penetration of protons, creates a distribution called a Bragg curve. The location of the Bragg peak is influenced by the materials placed on the paths of the protons. The Bragg peak is a bunch of very narrow monoenergetic proton beam in order to cover the total volume of the tumor. Bragg's peak can be widened by combining several beams with different energies, which are called Spread Out Bragg Peak (SOBP). Ocular tumors generally result in the spread of cancers in other parts of the body such as the lungs, prostate and abdomen which are called metastases. Although these tumors are introduced as secondary tumors, however the tumors such as melanoma and retinoblastoma are the main ocular tumors that develop and grow within the eye. Melanoma is the most common intraocular tumor that is more likely to develop in older ages. In 1974, Canstabel and Kohler discovered that the use of proton beams is appropriate for the treatment of tumors within the eye and can be focused on the tumor due to relatively high radiation doses. [2] In 1984, the Paul-Scherrer Institute in Switzerland began treatment for eye melanoma using 72 MeV proton beams and expanded its treatment program in 1996 using proton beams with energy of 200 MeV. [3] In 2006, Bernard used MCNP code to simulate the human eye and calculate the received dose. [4] In 2013, Dumbledot and et al., at the university of California, announced their research findings on 349 patients with eye melanoma. According to their report, proton therapy is beneficial for the treatment of melanoma, and the likelihood of vision after treatment is very high. [5] In 2015, Massoudi and et al., with eye simulating and placing the accurate eye compositions, showed that proton penetration is affected by the type of tissue compositions. [6] In 2017, Bakiyev and et al., investigated methods for reducing the radiation exposure of patients in the treatment room of eye diseases by radiotherapy [7] The ultimate goal of radiation therapy is to deliver a high dose of radiation to the tumor, while healthy tissues are not at risk of radiation. Because irradiation of healthy tissues increases side effects. A new strategy is to add nanoparticles to the tumor under radiation, which has been given over one decade in improving the function of conventional photon therapy. Several experiments provide sustained evidence of a significant increase due to the effects of ion radiation in the presence of nanoparticles. Meanwhile, these studies will help to identify possible mechanisms and predict the effects of ion beams and characteristics of nanoparticles. Many of the questions that have not yet been resolved can be partly addressed with the help of the study, and even the findings of this type of study can cause encourage and open new challenges. Gold nanoparticles (GNPs) have been suggested as a more effective criterion to improve the concentration of active products in the tumor and thus improve tumor targeting through radiation effects. When the tumor containing the nanoparticles is irradiated, the antibodies or peptides inside the tumor cells are affected. Therefore, a combination of radiotherapy with

nanomedicine opens up a new range of treatments. Therefore, new methods under investigation is increasing currently such that the dose is deposited at the site of the tumor, without damaging healthy adjacent tissues. The use of the combination of gold nanoparticles (GNPs) with high energy proton beams is a good potential for this. [8-11] While the effect of radiosensitivity may also be related to biological or chemical mechanisms, the physical interaction of radiation with GNPs is the main factor influencing the production of secondary radiation. This is due to the secondary radiation production of a low-energy in which it is deposited energy near GNPs and it causes the enhancement of localized dose. Monte Carlo simulations (MC) have been performed to measure the increased localized dose by many groups. [12-16] The interest in nanoscale simulations suggests a fundamental question; the choice of which physical interaction model can influence the predicted dose distribution around GNPs. Since charged particles, such as protons, are an important means in radiation therapy, yet unresolved physics issues prevent good performance of this method, including the estimation of deposited dose in non-homogeneous tissue, however this is an essential aspect of optimizing treatment.

GNPs are still under investigation for their ability to improve existing and develop new therapies. Reaching them is easy and can be used by various chemical methods. They are stable, non-toxic, non-immunogenic, and have resuscitation effects and high permeability on tumor cells. GNPs generation using the method of top-down is performed by applying the Nd: YAG laser by irradiation to a purified gold target embedded in the water. The laser characteristics are: 1064 nm or 532 nm wavelength, 3 ns pulse duration, 100 mJ pulse energy, 10 Hz repetition rate and 5 or 30 J/cm<sup>2</sup> fluence that can be used for realizing gold ablation with the laser. The gold by 10 ml of distilled water is immersed in a glass tube with about 20 ml water. The laser beam is deflected vertically by a prism and focused on the gold target. In general, the spot size is a circle with 0.5 mm<sup>2</sup> area, which corresponds to 20 J/cm<sup>2</sup>. During the repetition rate of irradiation, the target is moved in order to not ablate the same area and eliminate focal conditions. A solution of sodium citrate can be added to the solution of GNPs to prevent the coagulation of the nanoparticles with a minimum concentration of 1 g/ml. To improve their stability in biological solutions, GNPs can be combined with polyethylene glycol (PEG) peptides. In addition, GNPs can be functionalized with the different groups such as amine, carboxyl, peptide, DNA, RNA, antibody and be able to perform certain actions (adherence to the cell membrane, RNA carrier, targeting of cancer cells, and more). Peptides and proteins may be promising tools to improve the transfer of nanoparticles to cancer tissues. When NPs are injected compactly, they circulate throughout the body. More techniques are available for GNPs deposition in the cells of tumor. This liquid solution can be added by mechanical injection at the location of tumor, using a uniform distribution method as far as possible and preventing injection into vicinal healthy tissues. It can also be transmitted through the

bloodstream of these nanoparticles by injecting a solution containing GNPs under specific conditions into the blood vessels or by spraying it to the eye cancer tissue. NPs scam from the circulatory system to other tissues using endocytosis, shear forces, or passive diffusion through the pores network. In fact, nanoparticles with the size of less than 6 nm are driven out of the body by the kidney, while those greater than 6 nm are cleared by the liver.

For this purpose, in this article we study on the details of relativistics quantum physics of proton therapy .Therefore, in section 2, we discuss the Bethe-Bloch stopping power equation from a relativistics quantum view in detail.In section 3 , we investigate on the absorbed dose , range ,stragglng range, and mean Coulomb scattering angle. And in the section 4, we introduce an eye phantom that is used to calculate the absorbed dose via the Geant4 / Gate simulation. In Section 5, our numerical obtained results are described. Finally, we give a brief summary of our work.

**Quantum relativistic Bethe-Bloch model**

Stopping protons within the target is due to interactions between protons and atomic electrons. Since the mass of the proton is approximately 2000 times the mass of the electron, the path of the protons is not affected by much of these interactions. The amount of energy transferred in each interaction event between protons and electrons is associated with the proton being adjacent to the electron, and when the proton is stopped, this leads to an increase in energy transfer at the final stage, which is Bragg's peak for heavy charged particles. The stopping power equation of proton in a medium is given by Bethe-Bloch's quantum equation:

$$dE/dx=(nz^2 e^4)/(4\pi\epsilon_0^2 m_e v^2) [\{ \ln((2m_e v^2)/I) + [\Delta L]_{shell} + L_{Barkas} + \Delta_{LS} - \ln \ln(1-v^2/c^2) - v^2/c^2 - 1/2 + 2 \ln(1-1/\gamma^2) ]$$

Where z, is the atomic number of the heavy ion, e, is the electron charge, n is the number of electrons per unit volume of the medium, c is the speed of light in vacuum, is the ratio of ion velocity to the speed of light, I, is the average ionization potential energy, (0) is the vacuum permittivity coefficient and m\_e is the mass of the electron. [ΔL] shell is the shell correction and L Barkas , is the Barkas correction and Δ\_LS, is the Linard and Sorensen correction. The physical effects that this equation involves are:

**a) The effect of density**

The effect of the correction of the density that is involved in the process of stopping power is due to the effects of relativity, which reduces the stopping power in the material due to the polarization of the environment through the passage of charged particles. In dense targets, the electric field created by ions and electrons disturbs the proton path. Which is produced by the dielectric polarization of atoms. At high energies, the effects of the density correction is given by:

$$1/2 = -\ln(\epsilon) + \ln(1/(\hbar\omega)) + 1/2$$

where: β = V/C, γ=1/ (1-β²), and ħ is the reduced c

Planck constant, and ω is the plasma frequency.

**b) Shell effect**

A shell correction is due to the proton velocity, which is comparable to the electron velocities in the target atoms. This correction creates two issues, which are: 1. Proton velocity is sufficiently low compared to the internal electrons of shell atoms of target. 2. The inner shell electrons have sufficient relativistic velocities. The correction of the shell effect is given by ΔL<sub>Shell</sub> = -C/Z , in where C is obtained from the following equation:

$$C=(4.22377\Delta 10^{-7}) \beta^{-2} \gamma^{-2} + 3.04043 \times 10^{-8} \beta^{-4} \gamma^{-4} - 3.8106 \times 10^{-10} \beta^{-6} \gamma^{-6} ) I^2 + (3.858019 \times 10^{-9} \beta^{-2} \gamma^{-2} - 1.667989 \times 10^{-10} \beta^{-4} \gamma^{-4} + 1.57955 \times 10^{-12} \beta^{-6} \gamma^{-6} I^3) (3)$$

Which is valid for βγ > 0.13. I ,is the mean ionization potential energy of the target in eV, which indicates the amount of energy loss per unit length.

**c) Electron capture effect**

In a low-energy region (less than Mev 10), when the particle velocity is similar to one of the target electrons (≈ 0.0073c), ion neutralization due to electron capture plays an essential role in the stopping process, and z must be converted to Z\_eff: Z\_eff = z(1-exp (125 z²/3))) that was extracted from Barkas experimental data.

**d) Barkas effect**

The L<sub>Barkas</sub> term is known as Barkas correction. Barkas effect defines the effect of polarization within the target due to low energy collisions between protons and electrons. Subjectively, if the projectile is interacted with a harmonic oscillator, a correct factor 3pze²w/2m\_e v³ is obtained. Although effectively, it is recommended that this term be multiplied by logarithmic stopping ln(2m\_e v₂/ 1), so we have : L<sub>Baraks</sub> = 1+2z/v Z[F(V)] where: F(V)=0.0019exp(-2ln(V/10)) and V=βγ/α z is the reduced momentum. F(V) can not be used for v < 0.8.

**e) Lynard Sorensen (LS) Effect**

ΔL<sub>LS</sub> term in the stopping power equation is known as the Lyndard-Sorensen correction. Lynard Sorensen's correctin covers Bloch's correction at a low energy level and follows from the following relation which includes correction of relativistic scattering:

$$\Delta L_{LS} = \sum_{k=1}^{\infty} k/2 (k-1)/(2k-1) \sin^2(\delta_k - \delta_{k+1}) [k/(k+1) - 2k/(k+1) \sin^2(\delta_k - \delta_{k+1}) + 4k^2/(k^2+1) - 1/k] + \delta_k$$

where: γ = α z/ is a dimensionless parameter and =e²/(4 ε\_0 ħc), which is the hyperfine structure. δ\_k is Coulomb phase shift and K represents the quantum number of angular momentum.

**f) Nucleus finite size effect**

Nucleus finite size correction takes into account the physical size of the atomic nuclei within the target material. It is possible to obtain an accurate mathematical description for each symmetric spherical potential. This correction is moderately apparent for the Coulomb phase shift,  $\delta_k$ . This shift is a function of a parameter that provides a correction between the uniform spherical potential inside the nucleus and the outside of the coulomb potential. Now a standard function is introduced, which essentially represents the quantum mechanics of the perturbation:  $L_{stand} = \ln((2mv^2)/I \gamma^2) - v^2/c^2 - 1/2 \delta$ , where  $\gamma^2 = (1 - v^2/c^2)^{-1}$ . In addition,  $I$ , is determined by the Bethe relation:  $Z_2 \ln I = \sum_n f_{n0} \ln(h/\omega_{n0})$  and determined by the strength of the dipole oscillator ( $f_{n0}$ ) and  $\omega_{n0}$ , is the transition frequency. The  $-1/2 \delta$  function is similar to the fermi density correction effect, and its limit is large in collisions with high  $\sum$ . The  $L_{stand}$  function in the above equation depends only on the velocity  $V$  of the particle, the atomic number  $Z$  of the medium and the mean electron density, also, is independent on  $Z_1$  of the atomic number of particle. In fact,  $L_{stand}$  represents the theory of relativistic quantum perturbation, which implies that:  $dE/dx \sum Z_{12}$ . Thus, the first order of the quantum perturbation theory term is:  $L_{Pert} = L_{stand} + \sum ?L \int_{Shell}$

**2-1- The range and mass stopping power**

The mass stopping power can be determined from the relation:  $1/\sum S = -1/\sum dE/dx$ . Using proton stopping power and that protons lose their energy in a material continuously, and clinical proton beams contain millions or more of the accelerated protons as a result of interaction with the environment, so often the physical forms that describe them are inherently statistical. In this work, we use the CSDA method to calculate the proton range. The CSDA range is calculated by integrating on the initial and final energy of the incident particle divide to the inverse of total stopping power, which is given by:  $CSDA R = \sum_{E_f}^{E_0} dE / S$  Where  $E_0$  and  $E_{farc}$  the initial and final energy of the charged particle that is entered to the target, respectively. When a proton moves within a given material, it loses its kinetic energy due to various interactions. Finally, the particle is stopped. The distance that the particle travels is called the length of path. The distance that particle traverses to stop within the absorbent material is called the particle range. The absorbed dose is defined as the average energy is deposited in the environment per unit mass as a result of ionizing radiation. In SI system, the unit of the absorbed dose used in radiotherapy is Gy (1 Gy = 1 J / Kg) and is obtained from the following

equation:

$$D = 1.602 \times 10^{-10} \cdot F \cdot S / \rho \tag{6}$$

Where  $\rho$  is the density of the adsorbent material and the constant coefficient of  $1.602 \times 10^{-10}$ , converts MeV to Gy, and  $F$  is the number of charged particles (protons) per  $cm^2$ .

**Multiple Coulomb scattering**

Passing protons of matter may be deflected by the atomic nucleus, a process commonly referred to as scattering. More precisely, a multiple coulomb scattering can be seen when angular scattering occurs randomly due to the collective effect of many small single-scattering. Both the proton and the nucleus are positively charged, therefore, their interactions are mostly Coulombic. The Highland formula calculates the mean scattering angle  $\rho_0$ :

$$\rho_0 = 14.1 \text{ MeV/pv } z_p \sqrt{(L/L_R)} [1 + 1/9 \log_{10}(L/L_R)] \text{ rad} \tag{7}$$

where  $p$  is the proton momentum and  $v = c$ , is the proton velocity,  $L$  is the target thickness and  $L_R$  is the target radiation length. The radiation length is the distance which the energy of the radiation particles decreases due to radiation losses equal to the  $e^{-1}$  coefficient ( $\approx 0.37$ ).

**Geometry of the humann eye**

The geometry used in this paper represents the eyes of an adult human. The size and shape of the eye building are selected from published articles. [14-16] This geometry includes cornea, sclera, iris, lens, aqueous humour, vitreous humour, and optics nerve. The sclera is formed from the two cocenteric spheres was at radius of 1.2 cm and 1.1 cm with a thickness of 0.1 cm, and the cornea was made from two cocenteric spheres with radius of 0.78 cm and 0.65 cm. The eye lens is elliptic shape and the iris is placed in the form of two cylinders with a diameter of 0.62 cm between the cornea and the lens, the distance between the two cylinders being about 0.5 cm. The optic nerve is also cylindrical with a diameter of 0.25 cm and a height of 0.55 cm. The area between the cornea and the upper part of the lens is aqueous humour and the area between the lower lens and the sclera is vitreous humour. In fact, the inner part of the eye is filled with vitreous humour. The tumor is intended to be 4.3 mm within the eye, which is molded with 0.1 mm voxels to calculate the deposited energy. The main elements of each component of the eye and tumor are given in Fig. 1 and Table 1.

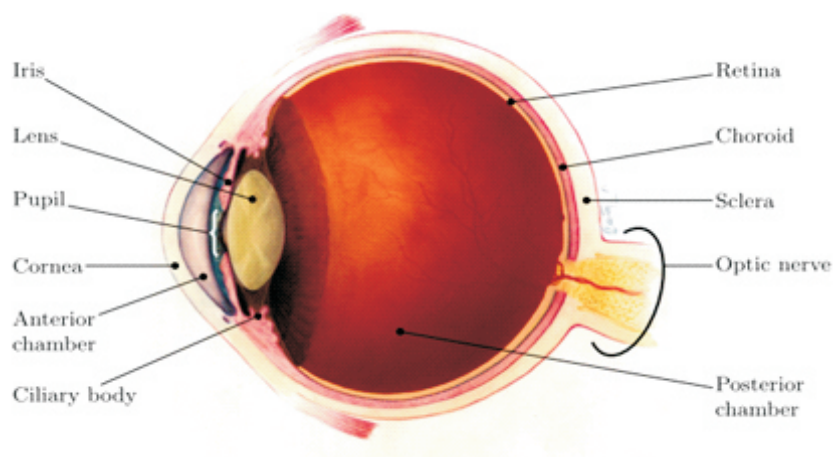


**Figure : 1** Anatomy of the humann eye.

**Table :1** The elemental composition and mass densities of some human tissues.

| Tissues         | $\rho(\frac{g}{cm^3})$ | H     | C     | N    | O     | Na   | P    | S    | Cl   | K    | Au  |
|-----------------|------------------------|-------|-------|------|-------|------|------|------|------|------|-----|
| Corona          | 1.050                  | 10.16 | 11.99 | 3.64 | 74.11 | -    | -    | 0.09 | -    | -    | -   |
| Scroll          | 1.050                  | 9.70  | 16.96 | 4.99 | 68.31 | -    | -    | 0.03 | -    | -    | -   |
| Vitreous humour | 1.0071                 | 11.09 | -     | -    | 88.04 | 0.38 | -    | -    | 0.45 | 0.03 | -   |
| Aqueous humour  | 1.0035                 | 11.10 | 0.10  | -    | 88.10 | -    | 0.3  | -    | 0.4  | -    | -   |
| Lens            | 1.070                  | 9.60  | 19.5  | 5.70 | 64.60 | 0.1  | 0.1  | 0.3  | 0.1  | -    | -   |
| Iris            | 1.050                  | 10.20 | 14.30 | 3.40 | 71.00 | 0.1  | 0.2  | 0.3  | 0.1  | 0.4  | -   |
| Tumor           | 1.040                  | 9.40  | 21.20 | 5.60 | 61.50 | 0.25 | 0.51 | 0.64 | 0.39 | 0.51 | -   |
| 10mgAu/ml       | 1.05                   | 10.6  | 14.4  | 2.2  | 70.5  | 0.2  | 0.4  | 0.2  | 0.3  | 0.3  | 1.0 |
| 25mgAu/ml       | 1.07                   | 10.4  | 14.2  | 2.1  | 69.5  | 0.2  | 0.4  | 0.2  | 0.3  | 0.3  | 2.3 |
| 50mgAu/ml       | 1.09                   | 10.2  | 13.8  | 2.1  | 67.9  | 0.2  | 0.4  | 0.2  | 0.3  | 0.3  | 4.6 |
| 75mgAu/ml       | 1.12                   | 10.0  | 13.5  | 2.1  | 66.4  | 0.2  | 0.4  | 0.2  | 0.3  | 0.3  | 6.7 |

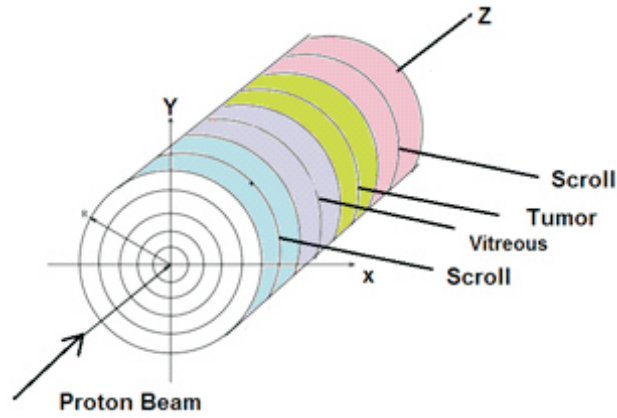


Figure : 2 Eye piece geometry in cylindrical shape .

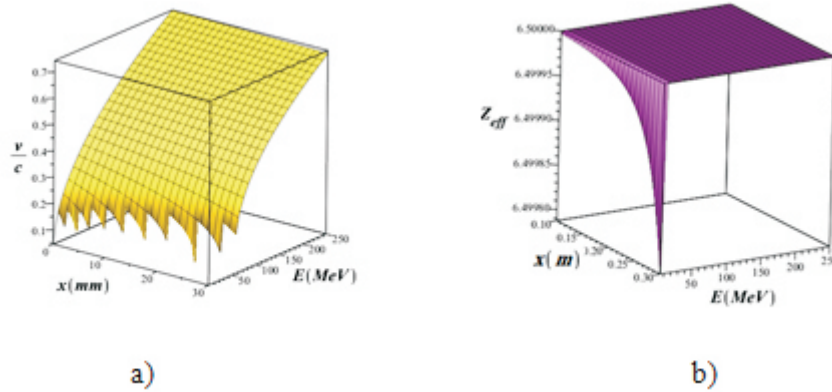


Figure : 3 3D variations of a)  $\beta=v/c$  and b)  $z_{eff}$  in terms of proton beam energy and the penetration depth in the eye tissue.

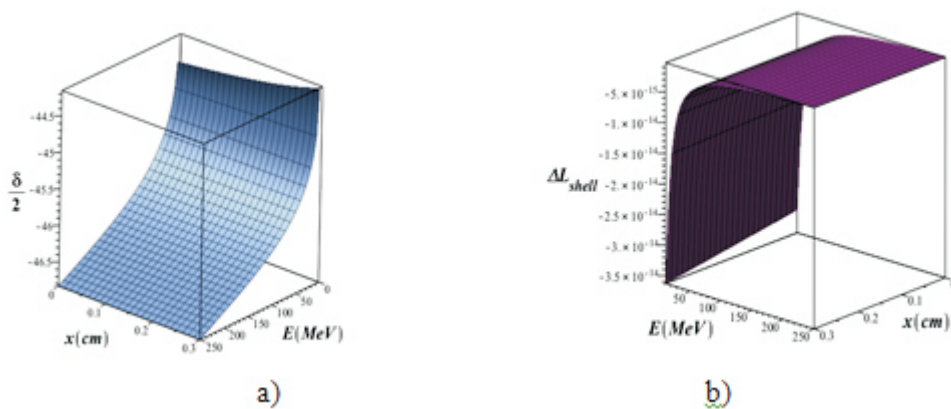
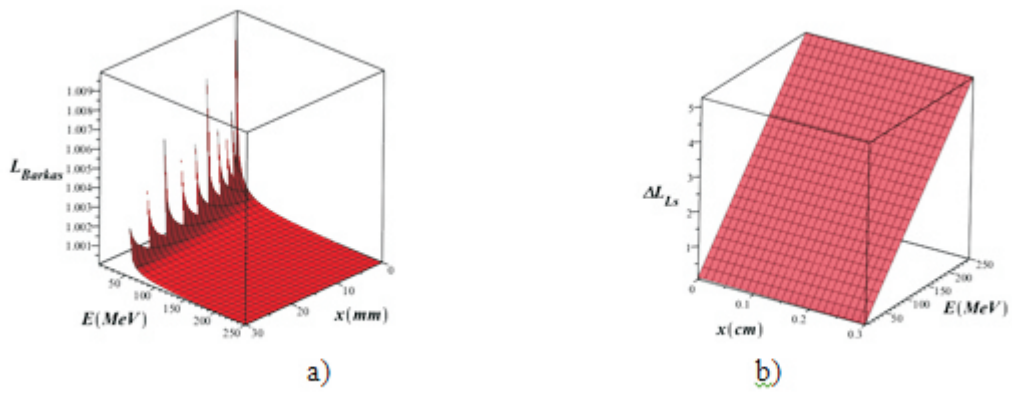
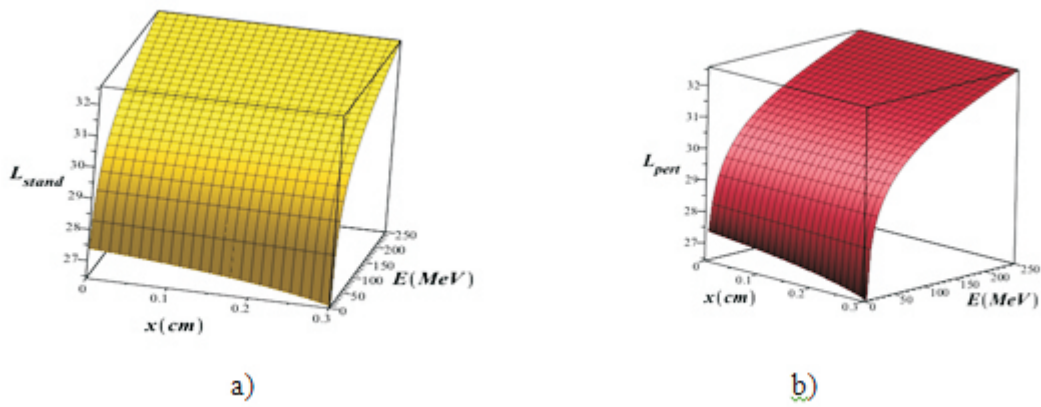


Figure : 4 Three-dimensional variations of a) density Effect ( $\delta/2$ ) and b) shell effect ( $\delta_{L\_shell}$ ) versus proton beam energy and penetration depth in the eye tissue.



**Figure : 5** Three-dimensional variations of a) Barkas effects ( $L_{Barkas}$ ) and b) Lyndard Sorensen  $\Delta L_{LS}$  ) effect in terms of proton beam energy and penetration depth in the eye tissue.



**Figure : 6** 3D variations of a)  $L_{stand}$  and b)  $L_{pert}$  as a function of proton beam energy and the penetration depth in the eye tissue.

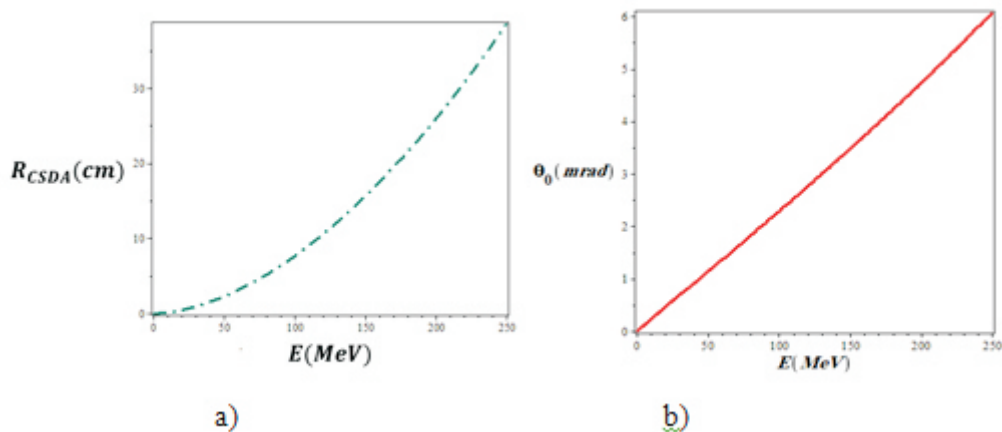


**Figure : 6** 3D variations of a)  $L_{stand}$  and b)  $L_{pert}$  as a function of proton beam energy and the penetration depth in the eye tissue.

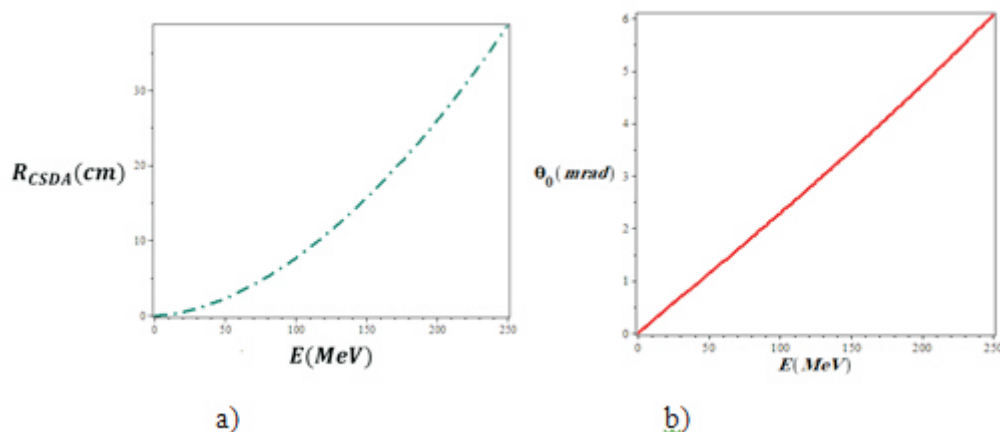


Figure : 7 3D variations of a)  $R_{CSDA}$  b)  $\Delta_0$  in terms of proton beam energy and penetration depth in the eye tissue.

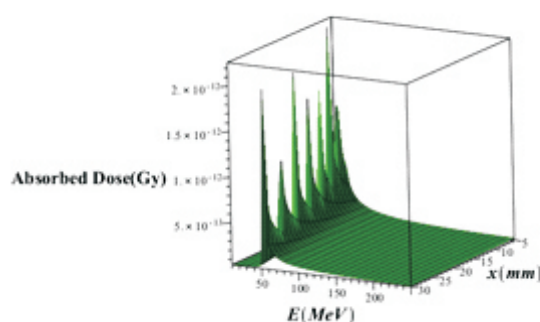
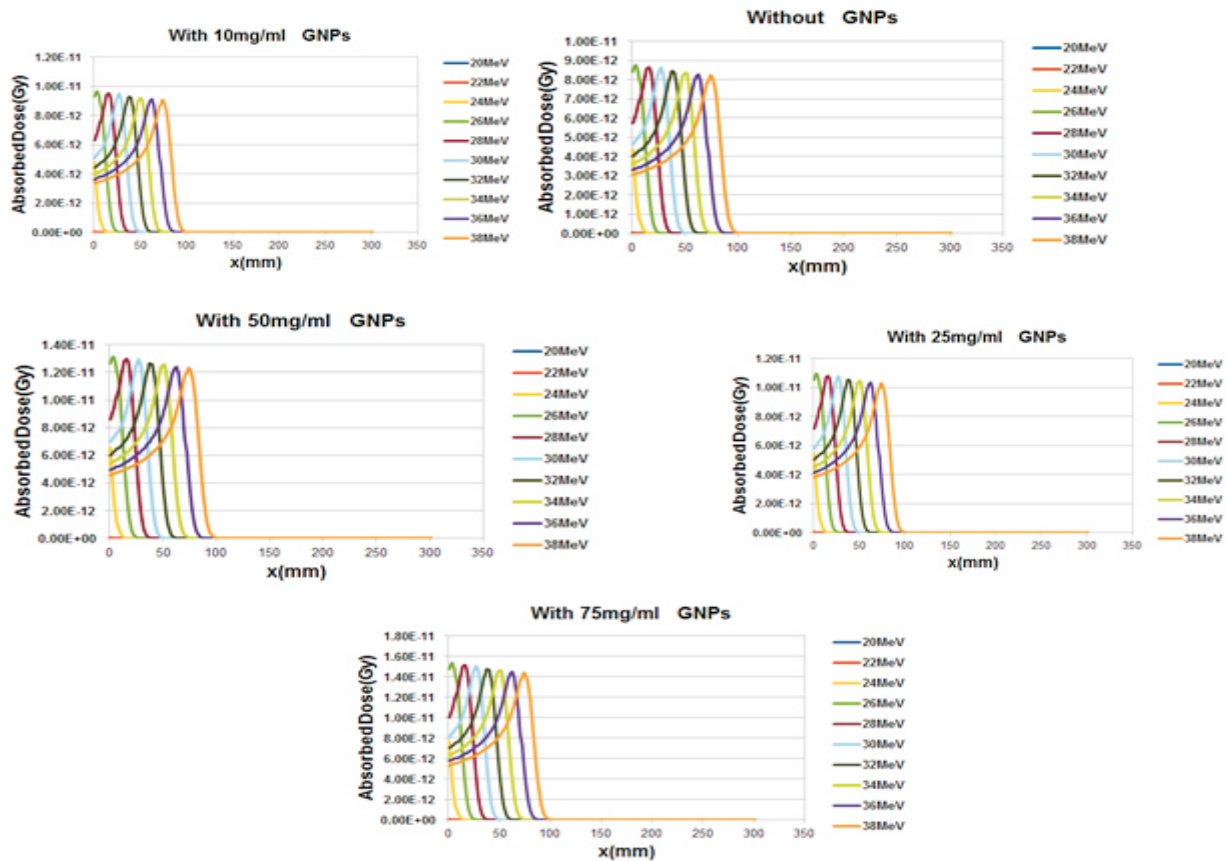


Figure : 8 Three-dimensional variations of absorbed dose calculated using the stopping power equation (1) in terms of proton beam energy and penetration depth in the eye tissue.

#### 4-1-Source and the piece geometry of eye

By changing the energy of the proton, we are trying to obtain optimal energy for the proton beam. The optimal energy is that the energy which the Bragg's peak created at this energy lies at the end of the tumor in the direction of radiation. To enhance the accuracy of the simulation and according to the irregular geometry of the eye, we simulate a cylindrical piece of phantom from the eye. Considering the position of the proton springs in the main geometry of the eye and according to the passage of protons from the layers of sclera, tumor and vitreous, the piece geometry is :the geometry consists of 4 cylindrical layers. The first and fourth layers are contained scroll with 0.15 cm long, the second layer includes tumor with length 30 cm, the third layer is vitreous with a length of 0.3 cm .This geometry is shown in Fig. 2. In this case, source is considered as a circular area , with a radius of 0.25 cm and located at a distance of 7 cm from the Z axis. Over the past few years, the use of computer science in the field of medical physics has become personalized and is rapidly increasing. Monte Carlo simulations are increasingly used for dosimetric purposes in PET, SPECT and CT diagnostic imaging methods (or therapeutic methods) for internal and external radiation therapy. At

present, the Monte Carlo method serves as the reference and standard code for dosimeters in clinical settings. In modern and personally-oriented medicine, measuring the absorbed dose or deposited energy is important due to the anatomical and physical changes of each patient. In imaging with ionizing radiation, assessing the absorbed dose in each organ or tissue intended to analyze cancer risks and assessing clinical protocols that increase the diagnostic and reducing effects of deliverable absorbing doses. In the area of radiation therapy, the distribution of an estimated absorbed dose due to various ionizing particles (electron, photon, carbon, and other radioisotope sources) plays a critical role in the treatment planning. Monte Carlo codes are widely used to simulate radiation physics and they are standard instruments for calculating electron transport and photon beams mainly in the field of radiotherapy and for dosimetric studies. MCNP is the standard code for radiation physics in the medical dosimetric field. In 2001, a code system for Monte Carlo simulations was published for the transfer of electron and photon pairs in arbitrary materials as well as complex quadrangle geometries. Two years later, CERN released the General Toolkit for the Geant4 simulation, a general Monte Carlo code related to physical processes that involves the particle collisions with matter.



**Figure : 9** Comparison of the absorbed dose in the suggested eye phantom with and without injection of gold nanoparticles in terms of penetration depth for different proton beam energy. (Nanoparticles of gold are considered in the form of a sphere with 50 nm diameter)).

Geant4 has been successful in the clinical and pre-clinical simulations which be the one of the strongest Monte Carlo reference codes in the field of medical physics. The use of Geant4 for the emission of computer tomography (GATE) is one of the high precision Monte Carlo tools in physical modeling and optimized for nuclear imaging applications. Compared to other Monte Carlo tools, the GATE provides more precision with regard to physical modeling, which is processed by Geant4 code and is widely used.

**Results and discussion**

In order to provide more complete physical concepts about the absorbed dose in eye cancer ,for the first time we calculated the behavior of the three-dimensional variations of all the terms in Equation (1) such as  $\beta$  parameter, the effective atomic number , $Z_{eff}$ , the density effect,  $\delta/2$ , the shell effect ,  $\rho L_{shell}$  ,Barkas effect , $L_{Barkas}$  ,Lynard Sorensen effect ,  $\rho L_{LS}$  , the standard perturbation function ,  $L_{stand}$  , the first order of general term of quantum perturbation theory , $L_{Pert}$  ,in terms of proton beam energy and depth of penetration in the eye tissue using Maple programming ,and the results are presented in Figures 1 through 6 In Figure 7 ,we plotted the two-dimensional variations of the CSDA range , $R_{CSDA}$  ,and

mean scattering angles ,  $\theta_0$  ,in terms of the energy of the proton beam .From this Figures ,it can be seen that  $R_{CSDA}$  and  $\theta_0$  increase with increasing the energy of the proton beam Also ,Figure 8 shows the variations of absorbed dose derived from the comprehensive theory presented in Equation 1 ,in terms of the proton beam energy and penetration depth in the eye tissue (using Maple programming .In Figure 9 ,absorbed dose in the eye tissue in terms of the proton energy in the range of 20 to 38 MeV with and without nanoparticles of gold nanoparticles at various concentrations of 10 ,25 ,50 and 75 mg / ml were plotted . (using Geant4 /Gate simulation )As it is seen ,by increasing the distance and energy from the beginning of the phantom , the magnitude of the absorbed dose in the Bragg 's peaks is reduced ,and the location of the Bragg peak moves with increasing energy to higher x and the lowest amount of absorbed dose is related to without injection of gold nanoparticles By increasing the amount of nanoparticles injection from 10 to 75 mg /ml ,the percentage of increasing absorbed dose for injection concentrations of 10 ,25 ,50 and 75 mg ml are equal to 1 .1 ,1 .25 ,1 .45 , 1 .75 and 1 .75 , compared to without injection of

nanoparticles of gold. This is due to the fact that high  $Z$  nanoparticles, such as nanoparticles of gold, increase the amount of deposited dose in the tumor or matter because of the increasing of secondary electrons and considering that the tumor is at a depth of 0.15 cm inside the phantom of the eye and its width is 0.99 cm, the optimum energy of the Bragg's peak is 26 MeV. According to the results of this work, the numerical value of the absorbed dose is confirmed by the Bethe-Bloch model and the Monte Carlo simulation model under Geant4 / Gate, but in the Monte Carlo simulation method under Geant4 / Gate, the height of the Bragg's peak gradually decreases with increasing the penetration depth of the proton within the tumor, while in the Bethe-Bloch method up to 50 MeV, the height of the Bragg peak does not decrease with increasing energy, but this has little effect on the absorption dose. The reason is that in the Geant4 / Gate simulation code instead of using Equation 1, the following equation is used:

$$dE/dx = (4\pi N_A z^2) / A (\rho r_e \rho^2 m_e c^2) / \beta^2 z^2 (\ln((2me v^2) / I) - \ln \rho (1 - \beta^2) - \beta^2 - C/Z)$$

but both methods still have numerical consistency.

## Conclusion

This work presents a study on the feasibility of using Gold-NPs to improve the efficiency of eye tumors. This study does not report clinical results in humans because, although Gold-NPs are non-toxic and have high permeability effects on tumor cells, further research is needed before use in humans. One of the potential limiting factors for the gold models available in the Geant4 nanoscale simulations is the fact that they are based on dense historical algorithms. Because of secondary electrons are produced from proton interactions, the development of more accurate gold models for the production of secondary electrons should be improved. As the Gate code has significant implications in the dosimeter which some of them are based on the Geant4 code, and others are related to the Gate itself, and in fact the Gate code has the high-level capabilities of Geant4 code in particle transport and geometry definition, and is based on time-dependent phenomena, this code uses more realistic simulations of these phenomena to determine absorbed dose. In this work we used the Monte Carlo simulation of the Gate code under Geant4 to calculate the absorbed dose using the proposed phantom for the treatment of the eye tumor, and we compared the obtained results with the results of a completely theoretical absorbed dose including quantum relativistic physics, and we confirmed the consistency between them. By simulating the piece phantom of the eye in the form of a cylinder and changing the energy of

the protons from 22 to 38 MeV and plotting the absorbed dose diagram in these energy range, the optimal energy is equal to 26 MeV, which in this energy of the Bragg peak is placed at the end of the tumor.

## References

- [1]. Dehghannia Rostami Z, Masoudi S.F, Asadi S. Dosimetry Comparison of Water Phantom and Complete Eye Definition for 125I and 103Pd Brachytherapy Plaques. *IJMP* 2011; 8(2):19-26. [Persian]
- [2]. Constable I. J, Koehler A. M. Experimental ocular irradiation with accelerated protons. *Invest Ophthalmology* 1974; 13(4): 280–287.
- [3]. Paganetti H. Proton Therapy: History and Rationale. In *Proton Therapy Physics*, New York: CRC Press:2012.
- [4]. Bernhardt D. Proton Dose Assessment to the Human Eye Using Monte Carlo N Particle Transport Code (MCNPX). *Health Physics*, Texas A&M University 2006; 1-73.
- [5]. Damato B, Kacperek A, Errington D, Heimann H. Proton beam radiotherapy of uveal melanoma. *Ophthalmology* 2013; 151-157
- [6]. Rasouli S.F, Masoudi S.F, Keshazare Sh, Jette D. Effect of elemental compositions on Monte Carlo dose calculations in proton therapy of eye tumors. *Radiat Phys Chem* 2015; 117:112-19.
- [7]. Bakaev V. A, Ivanov N. A, Lebedeva Z. S. Methods for reducing patient radiation exposure during proton therapy for eye disease. *St. Petersburg Polytechnical University Journal: Physics and Mathematics* 2017; 18-114:(2)3.
- [8]. Hainfeld J F, Slatkin D N and Smilowitz H M 2004 The use of gold nanoparticles to enhance radiotherapy in mice. *Phys. Med. Biol.* 49 N309–15
- [9]. Liu C-J et al 2010 Enhancement of cell radiation sensitivity by pegylated gold nanoparticles. *Phys. Med. Biol.* 55 931–45.
- [10]. Polf J C, Bronk L F, Driessen W H P, Arap W, Pasqualini R and Gillin M 2011 Enhanced relative biological effectiveness of proton radiotherapy in tumor cells with internalized gold nanoparticles *Appl. Phys. Lett.* 98 3–5
- [11]. Kim J-K, Seo S-J, Kim H-T, Kim K-H, Chung M-H, Kim K-R and Ye S-J 2012 Enhanced proton treatment in mouse tumors through proton irradiated nanoradiator effects on metallic nanoparticles. *Phys. Med. Biol.* 57 8309–23
- [12]. McMahon S J et al 2011b Nanodosimetric effects of gold nanoparticles in megavoltage radiation therapy *Radiother. Oncol.* 100 412–
- [13]. Leung M K K, Chow J C L, Chithrani B D, Lee M J G, Oms B and Jaffray D a 2011 Irradiation of gold nanoparticles by x-rays: Monte Carlo simulation of dose enhancements and the spatial properties of the secondary electrons production. *Med. Phys.* 38 624–31
- [14]. Wälzlein C, Scifoni E, Krämer M and Durante M 2014 Simulations of dose enhancement for heavy atom nanoparticles irradiated by protons. *Phys. Med. Biol.* 59 1441–58
- [15]. Lin Y, McMahon S J, Scarpelli M, Paganetti H and Schuemann J 2014 Comparing gold nano-particle enhanced radiotherapy with protons, megavoltage photons and kilovoltage photons: a Monte Carlo simulation *Phys. Med. Biol.* 59 7675–89
- [16]. Xie W Z, Friedland W, Li W B, Li C Y, Oeh U, Qiu R, Li J L and Hoeschen C 2015 Simulation on the molecular radiosensitization effect of gold nanoparticles in cells irradiated by x-rays *Phys. Med. Biol.* 60 6195–212.